Photodissociation and Vibrational Relaxation of OClO at Liquid Surfaces

Ilya Chorny, John Vieceli, and Ilan Benjamin*

Department of Chemistry, University of California, Santa Cruz, California 95064

Received: August 1, 2002; In Final Form: October 21, 2002

The photodissociation dynamics of OClO to O + ClO on the $^2A_2$ excited state and the vibrational relaxation of OClO in the ground electronic state at the interface of several polar liquids are studied using classical molecular dynamics computer simulations. The results are compared with recent calculations and experiments of photodissociation and vibrational relaxation of OClO in bulk water, acetonitrile, and ethanol. In contrast with substantial geminate recombination in the bulk, the photodissociation at the liquid/vapor interface of all three liquids gives rise to nearly 100% cage escape. In most of the trajectories at least one of the dissociation fragments desorb, although a significant percentage of the ClO fragments remain adsorbed at the interface. The reduced density at the interface gives rise to reduced friction and to slower vibrational relaxation of ground-state OClO (which may form as a result of geminate recombination of the photofragments). The vibrational relaxation of ground-state OClO is slower at the interface than in the bulk by a factor of 2−4, depending on the solvent and the excitation energy.

I. Introduction

The photodissociation of OClO to give (a) OCl + O, or (b) Cl + O_2, has been extensively studied in the gas phase[1−5] and in bulk liquids[6−21] due to its possible environmental impact.[22] These studies have contributed to the basic understanding of the nature of the excited-state potentials and the specific solvent−solute interactions that give rise to the observed quantum yield of the different photoproducts and the vibrational relaxation rate of the recombined OClO. These studies show that the O and ClO photofragments geminately recombine in water in less than 1 ps to give a ground-state OClO with a quantum yield of about 0.8. The geminate recombination yield is reduced by a factor of 6 when the photodissociation takes place in acetonitrile[17] and by almost a factor of 2 in ethanol.[20] The OClO formed undergoes vibrational relaxation that is approximately three time faster in water than in acetonitrile and ethanol.

While the experimental and theoretical studies have helped gain valuable insight into the bulk phase photochemistry of OClO, we lack basic knowledge about the photochemistry of OClO in other environments. A number of initial attempts to experimentally study this process at heterogeneous surfaces have been reported[23,24] with the goal of furthering our understanding of the factors that can influence the yield of different photoproducts. Study of this reaction at liquid interfaces is important for the above reason and to provide additional insight and a molecularly based understanding into the effect of different solvent properties on the observed geminate recombination yield and vibrational relaxation rate. In addition, a number of important photochemical reactions in the atmosphere are believed to occur at the surface of amorphous ice particles or at the surface of liquid droplets.

We have recently begun a systematic study of photodissociation and vibrational relaxation at liquid surfaces.[25−27] These studies focused on vibrational relaxation of polar and nonpolar diatomic solutes in water[26] and the photodissociation[25] and vibrational relaxation[27] of a nonpolar tri-atomic solute (ICN) in a nonpolar solvent (chloroform). Examining OClO at the surface of polar protic and aprotic solvents is an important extension of the above studies.

In two previous papers we reported our calculations on the vibrational relaxation[28] and photodissociation[29] of OClO in water, acetonitrile, and ethanol with results that are in good agreement with experiments. In this paper we discuss similar calculations carried out at the surface of these liquids with the goal of elucidating the role of the liquid interface region on vibrational relaxation and photodissociation of a polar molecule in polar solvents.

While the calculations in the bulk show significant probability for geminate recombination (in reasonable agreement with experiments), the photodissociation at the liquid/vapor interface of all three liquids gives rise to nearly 100% cage escape. We show that this is consistent with much slower vibrational relaxation at the interface, which minimizes the probability of the OClO to be trapped in the excited state. We also observe significant desorption of the oxygen and, to a lesser degree, the ClO photofragments. The vibrational relaxation of ground state OClO is strongly energy dependent and slower at the interface than in the bulk by a factor of 2−4, depending on the solvent and the excitation energy.

The rest of the paper includes in Section II a summary of the systems studied, the potential energy functions and the methods used to study the photodissociation and the vibrational relaxation. In Section III we discuss the results, followed by conclusions in Section IV.

II. Systems and Methods

In this section we discuss the potential energy functions and the methodology for conducting the photodissociation and the vibrational relaxation calculations at the liquid surface region. Each of the systems studied includes a single OClO molecule adsorbed at the liquid/vapor interface of one of the three solvents at 298 K. The shape of the simulation box is a parallelepiped whose size depends on the particular system and is listed in

* Corresponding author.

10.1021/jp021796m CCC: $25.00
Published on Web 12/10/2002

TABLE 1: The Systems Studied

the liquid	number of molecules	box dimensions (Å^3)
water	1024	$31.3 \times 31.3 \times 100$
acetonitrile	500	$35.1 \times 35.1 \times 100$
ethanol	500	$36.5 \times 36.5 \times 100$

Table 1. Three-dimensional periodic boundary conditions give rise to two liquid/vapor interfaces that are perpendicular to the long axis of the box (taken to be the *Z* direction). While OClO is a surface active molecule and tends to remain adsorbed at the interface, during a long simulation run it may diffuse to the bulk. For some of the molecular dynamics calculations, we employ a window potential, which prevents the molecule from escaping a 3 Å wide region centered at the Gibbs surface (the plane where the solvent density is 50% of the bulk value). This is simply done in order to increase the efficiency of data collection from the interface. Since the solute molecule does not interact with this potential when it is inside the window, this window potential does not affect any equilibrium calculations done at the interface. (The density profile of each of the three solvents and the probability distribution of the OClO center of mass will be discussed below.)

A. Potential Energy Functions. We briefly describe here the potential energy functions used in this work. For a more detailed description the reader should consult the previous papers devoted to the study of OClO in the bulk liquids.[28,29]

1. OClO Ground- and Excited-State Potentials. The ground X $^2B_1$ and the $^2A_2$ excited electronic states of OClO are given by a three-dimensional modified LEPS form which is fitted to ab inito multireference configuration interaction calculations by K. A. Peterson[30] in the Franck−Condon region. The ground-state dissociation energy of OClO ($D_0 = 59$ kcal/mol), data from photofragment translational energy spectroscopy experiments,[3] and information about the potential energy functions of O_2 [31] and ClO[32,33] are used as constraints in the fit. The potential is given explicitly by

$$U_{\mathrm{OClO}}(r_1,r_2,r_3) = U_{\mathrm{LEPS}}(r_1,r_2,r_3) + ke^{-\alpha(r_1+r_2)}(r_3 - r_3') + k_1 e^{-\beta[(r_1-a)^2+(r_2-a)^2]}$$

$$U_{\mathrm{LEPS}}(r_1,r_2,r_3) = Q_1 + Q_2 + Q_3 - [0.5(J_{23}^2 + J_{13}^2 + J_{12}^2)]^{1/2}$$

$$Q_i = 0.5D_{1i}[(e^{-\beta_{1i}(r_i-r_{1i})} - 1)^2 - 1] + 0.5D_{3i}[(e^{-\beta_{3i}(r_i-r_{3i})} + 1)^2 - 1]$$

$$J_{ij} = J_i - J_j \quad i,j = 1,2,3 \quad i \neq j$$

$$J_i = 0.5D_{1i}[(e^{-\beta_{1i}(r_i-r_{1i})} - 1)^2 - 1] - 0.5D_{3i}[(e^{-\beta_{3i}(r_i-r_{3i})} + 1)^2 - 1] \quad (1)$$

where r_1 and r_2 are the two O−Cl bond lengths, r_3 is the O−O distance, and r_3' is the O−O distance at the equilibrium OClO bend angle ($r_3' = \sqrt{r_1^2 + r_2^2 - 2r_1r_2\cos\theta_{\mathrm{eq}}}$). More details about these potentials including plots showing the quality of the fit to the ab inito data and the value of all the parameters for the ground- and excited-state potentials can be found elsewhere.[29] An important feature of the excited-state potential is the existence of a late barrier to dissociation along the asymmetric stretch of OClO. This barrier is around 12 kcal/mol near the equilibrium OClO bond lengths, in agreement with estimates based on photofragment translational spectroscopy experiments.[3]

2. Liquids' Potential Energy Functions. The liquid potentials used in this work have been shown to give reasonable structural, thermodynamic, and dynamic properties of bulk water,[34] bulk liquid acetonitrile,[35] and bulk ethanol.[36] These potentials include an intramolecular part (which is necessary when studying photodissociation and vibrational relaxation processes in liquid) and an intermolecular part. The liquid intramolecular potential energy function for water is the spectroscopic potential of Kuchitso and Morino.[37] The intramolecular potential for CH_3-CN is modeled using a harmonic force field for the CC and CN stretches and the CCN bend whose parameters are selected to reproduce the fundamental vibrational frequencies of gas-phase CH_3CN.[38] For ethanol, the intramolecular potential energy function includes harmonic bond stretches, harmonic angle bends, and a three-term Fourier series for the CCOH torsional mode. The CH_3 and CH_2 groups in ethanol and the CH_3 group in acetonitrile are treated as united atoms with the appropriate mass of these groups.

The intermolecular part of the potential is modeled as a pairwise sum of Lennard-Jones + Coulomb terms:

$$U(\mathbf{r}) = \sum_{i<j} 4\epsilon_{ij}\left[\left(\frac{\sigma_{ij}}{r_{ij}}\right)^{12} - \left(\frac{\sigma_{ij}}{r_{ij}}\right)^{6}\right] + \frac{q_iq_j}{r_{ij}} \quad (2)$$

where r_{ij} is the distance between atomic sites i and j (in two different molecules), q_i and q_j are the fixed charges on sites i and j, and the Lennard-Jones parameters σ_{ij} and ϵ_{ij} are determined from the parameters of the individual sites according to the usual combination rules for mixtures:[39]

$$\sigma_{ij} = \frac{1}{2}(\sigma_i + \sigma_j),\ \epsilon_{ij} = \sqrt{\epsilon_i\epsilon_j} \quad (3)$$

The choice of the parameters q_i, σ_i, and ϵ_i for the water atoms follows the original SPC model.[40] For CH_3CN, the parameters are taken from the work of Edwards, Madden and McDonald[35] and, for C_2H_5OH, from the work of Jorgensen.[36] All of the intermolecular and intramolecular parameters used in the present work are listed elsewhere.[41,42]

3. OClO-Liquid Potential Energy Functions. The interaction potentials between each of the three liquids and the OClO in the ground and excited states are also modeled using a Lennard-Jones plus Coulomb terms between each of the OClO atoms and each site on the liquid molecules. The Lennard-Jones parameters are determined using the combination rule for mixtures (eq 3) and the following parameters for the O and Cl sites in the OClO:

$$\sigma_{\mathrm{O}} = 3.16\ \text{Å},\ \epsilon_{\mathrm{O}} = 0.155\ \text{kcal/mol}$$

$$\sigma_{\mathrm{Cl}} = 3.5\ \text{Å},\ \epsilon_{\mathrm{Cl}} = 0.348\ \text{kcal/mol}$$

For simplicity and in order to be consistent with our bulk liquid calculations, we assume that the Lennard-Jones parameters for the excited state are the same as that for the ground state.

The charges on the OClO atoms in the ground and excited states depend on the geometry of the molecule. In the Franck−Condon region these charges are determined from the ab initio calculations mentioned above. As the OClO dissociates, the charges on the atoms change, approaching the asymptotic values appropriate to the products O + OCl which are determined from the dipole moment of OCl. We approximately handle this feature of the system by using a simple switching function, which makes

each of the charges on the OClO atoms dependent on the degree of the dissociation according to

$$q_\nu = q_\nu^\infty + \frac{q_\nu^{eq} - q_\nu^\infty}{1 + \gamma\rho^2} \quad (4)$$

where $\rho = r_1^2 - r_2^2$ (r_1 and r_2 are the two O−Cl bond lengths) is our choice for the reaction coordinate for the dissociation reaction and ν stands for each of the three OClO atoms. The values of all the parameters used in eq 4 can be found elsewhere.[29]

While the classical model described above is highly approximate and cannot describe all aspects of the photodissociation process, it nevertheless was quite helpful in providing some molecular insight into the photodissociation of OClO in bulk liquids. Using this model to discuss the photodissociation of OClO at the liquid/vapor interface of the same liquids is therefore a reasonable first step in trying to understand this complex system

B. Methods. *1. Absorption Spectra.* The electronic absorption spectrum is determined using the classical Franck−Condon approximation:

$$I_{abs}(\omega) = \omega(1 - e^{-\hbar\omega/kT})\langle|\mu(\mathbf{r})|^2\delta[\omega - \Omega(\mathbf{r})]\rangle_g \quad (5)$$

where $\mu(\mathbf{r})$ is the electronic transition dipole moment as a function of the nuclear positions $\mathbf{r}$. The ensemble average in eq 5 is over the ground state, (determined from a 200 ps equilibrium trajectory) and $\hbar\Omega(\mathbf{r}) = U_{ex}(\mathbf{r}) - U_{gr}(\mathbf{r})$ is the energy gap between the excited-state and the ground-state potentials at each nuclear configuration. For simplicity, we take the electronic transition dipole moment $\mu(\mathbf{r})$ to be a constant.

2. Photodissociation Calculations. The trajectory used to compute the spectrum is also used to select 40 independent configurations, which obey the classical Franck−Condon condition for an excitation with a 350 nm light. This is done by integration of the classical equation of motion on the ground electronic state and a search for configurations for which $\hbar\omega = V_{ex}(\mathbf{r}) - V_{gr}(\mathbf{r})$ for the given photon energy. (For other methods see reference[43] and references therein). Each of the independent Franck−Condon initial configurations is used as a seed to generate 10 trajectories using different initial velocities selected from a Boltzmann distribution at 298 K, resulting in a total of 400 independent trajectories. All the molecular dynamics calculations are done using a time step of 0.5 fs and the velocity version of the Verlet algorithm

It is important to point out that the above model does not take into account the existence of multiple OClO excited states, such as the $^2B_2$ and the $^2A_1$ states. While much of the gas-phase experimental data can be explained by assuming that the excited-state dynamics is dominated by motion on the $^2A_2$ excited state[3] (used here), there is also some evidence that transitions from the $^2A_2$ to the $^2A_1$ state are important for the understanding of OClO photochemistry in the condensed phase[15] and for elucidating the mechanism for the formation of the ClOO isomer.[18]

3. Vibrational Relaxation. The vibrational relaxation calculations are performed by exciting an adsorbed OClO molecule to an initial vibrational energy which is selected from uniform grid points in the two ClO bond lengths. This places the excitation energy in a combination of the symmetric and anti-symmetric mode, in qualitative agreement with what is believed to be the initial distribution of the vibrational energy following the geminate recombination of the O and the ClO fragments (from kinetic analysis of Stokes and anti-Stokes intensities[16]). The same approach has been used in the calculations done in the bulk liquids.[28] A total of 320 trajectories divided into four groups according to their initial excitation energy were run. The length of each trajectory depends on the solvent and will be reported below. The OClO molecule remains in the interface region during the entire length of each trajectory. The quantity of interest we calculate is the time-dependent ensemble average of the OClO vibrational energy:

$$C(t) = \frac{\bar{E}(t) - \bar{E}(\infty)}{\bar{E}(0) - \bar{E}(\infty)} \quad (6)$$

where $\bar{E}(t)$is the ensemble average of the energy at time t.

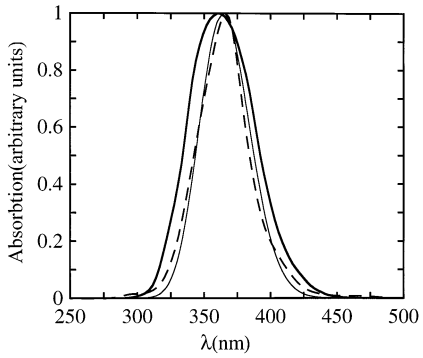

Figure 1. The absorption spectrum of OClO in bulk water (thick line), at the liquid/vapor interface of water (thin line), and in the gas phase (dotted line).

III. Results and Discussion

A. Absorption Spectra. The calculated electronic absorption spectrum of OClO at the surface of water compared with the spectrum calculated in the bulk and in the gas phase is shown in Figure 1. The calculated spectrum in bulk water is in reasonable agreement with the experimental one, as discussed elsewhere,[29] and it is only slightly shifted to the blue relative to the gas phase. This is due to the smaller electric dipole moment of OClO in the excited state ($\mu = 1.75$ D) than in the ground state ($\mu = 1.85$ D). This shift is even smaller at the interface due to the reduced polarity of water in this region.[44,45] The calculated spectrum of OClO in bulk acetonitrile and ethanol was shown to be almost identical to the one in bulk water[29] (in agreement with experiments[14,20]), and the same is true at the interface and thus it is not reproduced here. The small shift between the bulk and the interface reflects both the weak solvent−solute interactions and the small change in the dipole moment between the ground and the excited states of OClO.

B. Photodissociation of OClO at the Liquid/Vapor Interface. The inserts in Figure 2 depict the initial probability distribution function of the position of the OClO center of mass along the interface normal superimposed on the liquid's density profile. This distribution is centered at the Gibbs surface with tails that reach 1.5 Å on each side. While this suggests that OClO is a surface active molecule, free energy calculations are required to obtain a quantitative adsorption free energy. This knowledge, however, is not required for the calculations described below. Following the 350 nm excitation, the OClO is placed on the short-range repulsive part of the excited-state potential with an energy that is approximately 24 kcal/mol above the asymptotic O + ClO region and about 12 kcal/mol above the barrier along the asymmetric mode. In principle, the O and ClO photodissociation fragments can stay at the interface, diffuse to the bulk, or desorb into the gas phase. Figure 2 gives the

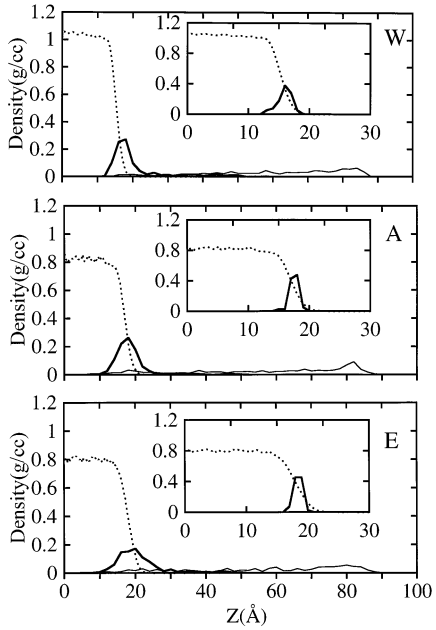

Figure 2. Density profiles (dotted lines) of water (W), acetonitrile (A), and ethanol (E), and the probability distribution of the positions of the O (thin line) and the ClO (thick line) photofragments at the end of the 10 ps trajectories. The insert in each panel shows the equilibrium probability distribution of the OClO center of mass prior to photoexcitation.

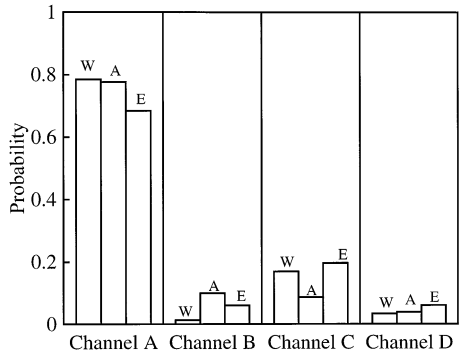

Figure 3. Probability of observing the O and OCl photodissociation fragments in the four different channels following dissociation of OClO at the liquid−vapor interface of water (W), acetonitrile (A), and ethanol (E). In channel A, the oxygen desorbs and OCl remains adsorbed at the surface, in channel B both fragments remain adsorbed, in channel C both fragments desorbed, and in channel D the OCl desorbs and the oxygen remains adsorbed at the surface.

probability distribution of the location along the interface normal of the two photofragments at the end of the 10 ps trajectory and can be used to determine the fraction of trajectories that end up in each of the possible channels. Since during the first 10 ps following the photodissociation, a negligible fraction of the photofragments diffuses to the bulk, we focus on those four channels that include: (A) O desorbs and OCl remains adsorbed at the surface, (B) both fragments remain adsorbed, (C) both fragments desorbed, and (D) OCl desorbs and O remains adsorbed at the surface.

Figure 3 summarizes the probability of finding the O and OCl photofragments in the above four channels. In all three liquids, the major channel is channel A (probability between 0.8 and 0.7). This is not surprising since the lighter oxygen atom carries about 75% of the translational energy available to the two fragments which makes it easy for this weakly solvated species to desorb. For this same reason, the least probable channel is the one where the OCl desorbs while the O remains

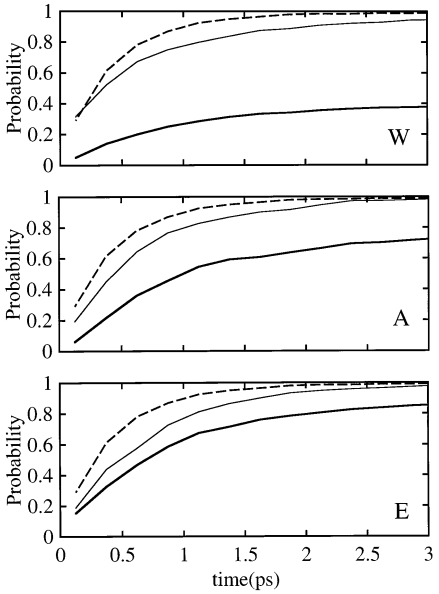

Figure 4. Cumulative probability distribution of dissociation times following the 350 nm excitation of OClO in water (W), acetonitrile (A), and ethanol (E). In each panel, the thick solid line and the thin line correspond to trajectories run in the bulk or the interface, respectively. Each panel also contains the results for trajectories run in the gas phase (dashed line).

at the surface (channel D). Somewhat more surprising is the observation that the second most populated channel (probabilities in the range of 0.2−0.1) is the one where both fragments desorb (channel C). These results make more sense when one examines the probability distribution of the OCl bond orientation at the moment of dissociation (data not shown). The trajectories which involve OCl desorbing from the surface have on average their Cl atom pointing toward the vapor phase, while the trajectories which involve O desorption, the OCl bond orientation is completely random. The most interesting point about the data shown in Figure 3 is the very close similarities in the populations of the four channels among the three liquids: despite the different interaction between the fragments and the three liquids (which is shown to have important consequences for some other properties discussed below), their probability of desorption is determined by such factors as the mass of the fragments and the molecular orientation, but not the nature of the solvent.

As discussed elsewhere,[29] the initial dynamic of OClO atoms on the excited state is along the symmetric mode. This is due to the fact that the Franck−Condon region of the excited state potential is where the intramolecular forces are directed along the symmetric stretch. Since the motion along this mode is bounded, there is a time delay to dissociation during which the molecule vibrates along the symmetric mode until its intramolecular motion places it along the antisymmetric mode. At this time the molecule dissociates if it has enough energy to go over the barrier. If we define the dissociation time to be the time at which the trajectory crosses the barrier without turning back, we arrive at the distribution shown in Figure 4. What is in fact shown is the cumulative probability distribution of dissociation times which is also compared with the results in the bulk of each liquid and in the gas phase. The most obvious result depicted by Figure 4 is that while in the bulk liquid only a fraction of the trajectories dissociate by going over the barrier and escaping the cage, this fraction is very close to 100% in all the three liquid surfaces and its time-dependent shape is very similar to the one calculated in the gas phase. To understand

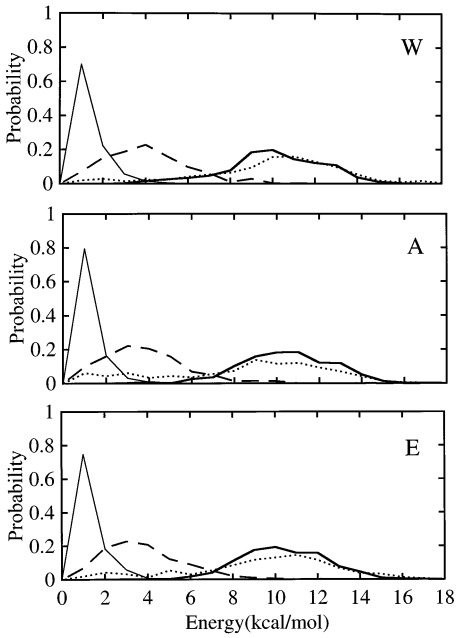

Figure 5. Energy distribution in the O and ClO photofragments following photodissciation of OClO at the liquid/vapor interface of water (W), acetonitrile (A), and ethanol (E). The distributions are computed at the moment in each trajectory when the OClO dissociates (see the text for an exact definition). Solid thick line: ClO vibration; solid thin line: ClO rotation; dashed line: ClO translation; dotted line: O translation.

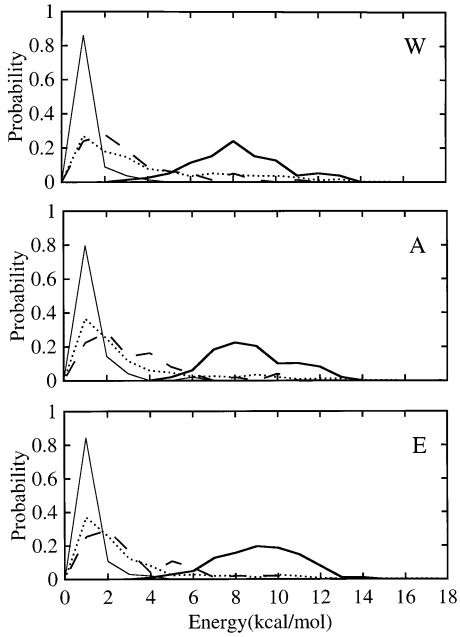

Figure 6. Same as Figure 5 except that the energy distributions for each of the dissociation fragments are calculated when this fragment desorbed from the surface.

this, note that most of the trajectories dissociate in the first 1−2 ps following excitation (and in less than 1 ps in the gas phase in agreement with recent experiments[2,3]). During this time while the OClO is "searching" for the exit channel along the antisymmetric mode, energy relaxation to the liquid depletes the amount of energy available to the OClO to climb over the barrier located along the antisymmetric mode. As will be shown below, the rate of vibrational relaxation at the interface is much slower than in the bulk. This leads to trapping in the excited state of a significant fraction of the bulk phase trajectories, while nearly 100% dissociation occurs at the interface. (OClO trapped in the excited state will relax to the ground state via radiationless transitions, which are not included in our model). Indeed, because the rate of vibrational relaxation in water is much greater than in the other two liquids,[28] the fraction that dissociate (and thus cage escaped) in bulk water is smaller than in ethanol and in acetonitrile as is clear from the thick lines in Figure 4. Thus, Figure 4 suggests that geminate recombination will be quite similar at the surface of these three liquids and much smaller than in the bulk where they are 80−83% in water,[16,21] 14−22% in acetonitrile,[17,21] and 50% in ethanol. Finally, examination of the short time ensemble average of the OClO potential energy as well as single individual trajectories (not shown) clearly demonstrates that the initial intramolecular dynamics in OClO involves damped oscillation along the symmetric mode which are nearly solvent-independent, explaining the similar (bulk vs interface) early time behavior in Figure 4.

We turn now to a discussion of the energy disposal into the photodissociation fragments. Figures 5 and 6 show the energy distribution into different modes at two different time points during the photodissociation process. In Figure 5 we show the oxygen atom translational energy distribution and the OCl translational, rotational, and vibrational energy distribution after the photofragments crossed the barrier in the excited state and reached the point where the energy difference between the ground and excited state is less than a *kT*. At this point in time (which is different for different trajectories), all degrees of freedom carry significant energy except OCl rotation, which is consistent with gas-phase experiments.[3] The energy disposal into the different modes reflects the initial conditions and the detailed intramolecular dynamics on the excited state and thus is very similar when OClO dissociates at the surface of the three liquids. As indicated earlier, the average energy in the O translational motion (11 kcal/mol) is about a factor of 3 larger than in the OCl translation (corresponding to the mass ratio of these two fragments).

In Figure 6 we present the same distribution at the time when each fragment desorbs from the surface, defined as reaching the plane $Z \geq 25$ Å. (This time is again different for different trajectories.) Thus, the distributions of the OCl energies involve ensemble average of trajectories which belong to the C and D channels. Comparison with Figure 5 shows that while the OCl and O fragments experienced a significant translational cooling, many are still desorbing with above thermal translational energies. In contrast, there is almost no change in the degree of OCl vibrational excitation and this diatomic molecule is still vibrationally hot upon desorption, reflecting slow interfacial vibrational relaxation (see below).

Figure 7 completes the discussion of the energy disposal in the photofragments by showing the ensemble average of the OCl translational, rotational, and vibrational energy and the oxygen atom translational energy in the case where the photofragments remain at the surface. This figure underscores the fast rotational and translational energy relaxation and the slow vibrational relaxation at the interface. In separate calculations[26] we have found that the vibrational relaxation time of OCl at the liquid/vapor interface of water is 28 ps which is much slower than in bulk water (8 ps), while in bulk acetonitrile and ethanol the rate is slower than 100 ps and thus expected to be even slower at the interface. The OCl is a relatively high-frequency oscillator[32] (859 cm^{-1}) and thus it is not surprising that it relaxes relatively slowly in water and very slowly in the other two liquids.

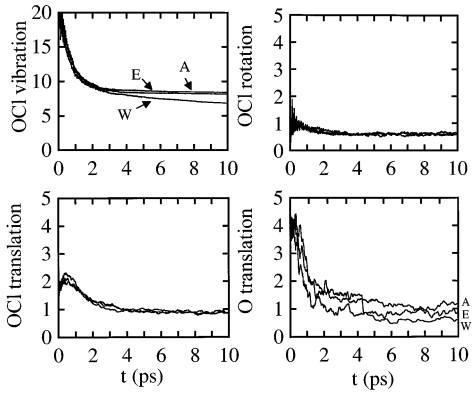

Figure 7. Time-dependent ensemble averages of the O and OCl photofragments energies (kcal/mol) for the fragments that remained at the interface following dissociation of OClO at the liquid/vapor interface of water (W), acetonitrile (A), and ethanol (E). Note the different energy scale in the panels. No labels are given when the three different lines nearly overlap.

The rate of OCl translational relaxation is about a factor of 2 slower than that in the bulk and is nearly independent of the solvent. Based on Figure 7 we estimate the rate to be 1 ps in bulk water[29] compared with 2 ps at the interface, reflecting the fact that only a few collisions with the solvent molecules are sufficient for relaxation and the frequency of these collisions at the interface is lower. The noisy plot of the oxygen atom translational relaxation is due to the small number of trajectories in which the oxygen remains at the surface (channels B and D accounting for about 10% of all the trajectories). Nevertheless, this plot also shows fast relaxation (near 4 ps) that is only slightly slower than in the bulk liquid (around 3 ps[29]). The slower relaxation of the oxygen translation compared with the ClO translation is consistent with the simple kinematic idea that the efficiency of translational energy transfer increases when the colliding particles have similar masses. This also explains the similar behavior of the three liquids (the hydrogen bonding network in water gives rise to a larger effective mass than the 18 au of a single water molecule).

To conclude this section it is useful to compare the results presented here with a recent study of the photodissociation of ICN at the liquid/vapor interface of chloroform.[25] In this case, both the solute and the solvent are nonpolar, yet we find that this system exhibits many similarities with the systems examined in the present work. In particular, in all systems there is a dramatic increase in the probability of cage escape relative to the bulk liquid and significant desorption of the photofragments that is asymmetric (i.e., one of the photofragments is much more likely to desorb). The desorption probability is correlated with the amount of translational energy available to the fragments (which is determined by their mass ratio) and their initial orientations. The differences that do exist can be traced to differences in the solute potential energy functions and photofragment masses and not the liquids.

C. Vibrational Relaxation of OClO at the Liquid/Vapor Interface. The above calculations suggest that most of the photofragments produced by photodissociation of OClO on the $^2A_2$ excited state at a liquid surface do not have an opportunity to recombine on the ground state. The large translational energies enable the fragments to escape the relatively small degree of caging that exists at the liquid surface. However, our model does not take into account the existence of several other excited states that could lead to an early transition to the ground state. Indeed, recovery of ground-state OClO is observed experimentally during the first 1 ps following excitation,[15] which suggests that some of the ground state OClO is formed by a mechanism which does not involve the relatively slower dissociation along the $^2A_2$ excited state. Thus, photodissociation at a liquid surface may produce vibrationally excited ground-state OClO molecules whose subsequent relaxation is the focus of this section.

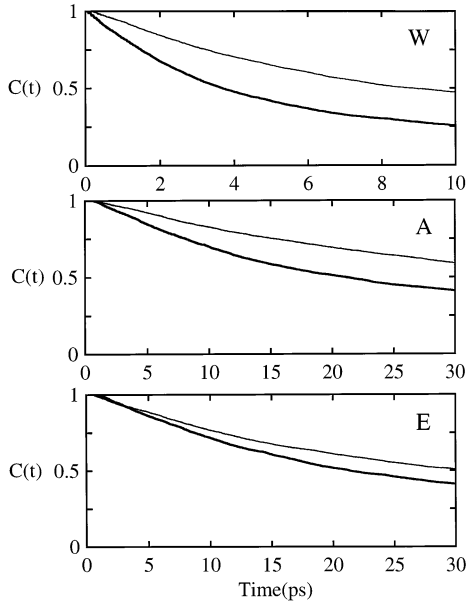

Figure 8. Normalized nonequilibrium energy relaxation following vibrational excitation of OClO at 298 K at the liquid/vapor interface of water, ethanol, and acetonitrile. In each panel the thick line represents the results in the bulk liquid and the thin line at the liquid/vapor interface. Note the different time-scale in the top panel.

TABLE 2: Nonequilibrium Energy Relaxation Times (ps) of OClO in Different Environments

	molecular dynamics results					
average excitation energy (kcal/mol)	7	18	30	37	overall average	exptl values[a]
bulk H_2O	13.4	9.2	6.1	4.4	6.4	9
surface H_2O	48.3	23.4	12	8.5	11.6	
bulk CH_3CN	82.4	62.6	26.5	20.2	31.9	37 ± 12
surface CH_3CN	317	136	45.6	39.8	55.6	
bulk C_2H_5OH	84.1	70.2	25.4	19.2	30.4	31 ± 10
surface C_2H_5OH	162	136	34.9	29.8	41.7	

[a] Experimental and calculated bulk values are taken from ref 28.

While the above calculations and other calculations[29] and experiments[16] in bulk liquids indicate that the initial motion of the OClO is along the symmetric stretch, intramolecular dynamics on the excited state give rise to a rapid development of dynamics along both the symmetric and anti-symmetric modes (indeed, the dissociation on the $^2A_2$ state requires motion along the anti-symmetric stretch.) It is reasonable to expect that vibrationally hot OClO will be produced with significant energy in both of these modes. Thus, our vibrational energy relaxation calculations are done with initial energy distributed in both modes as explained in detail in Section II.3 above.

Since the OClO dissociation energy in the ground electronic state is 59 kcal/mol, we have examined several different initial excitation energies below this value. Figure 8 compares the average relaxation (shown as the normalized nonequilibrium correlation function defined in eq 6) over all of the above initial conditions, in each of the three liquid surfaces and in the bulk. Table 2 gives the corresponding relaxation times (from a single-exponential fit) as well as the individual rates calculated for each of the different excitation energies.

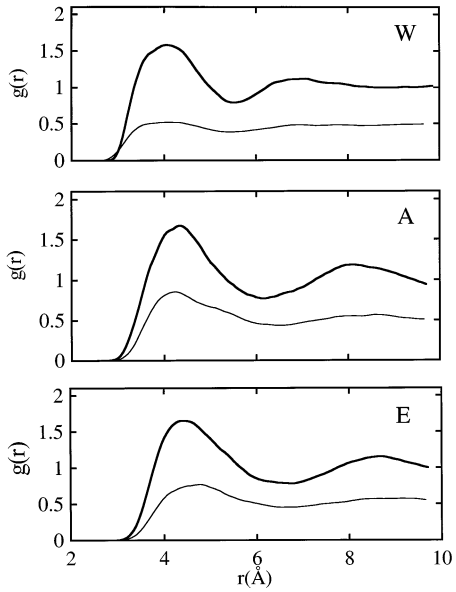

Figure 9. Radial distribution function of OClO in the bulk (thick solid line) vs the liquid/vapor interface (thin solid line). In each panel, the distribution function is for the Cl atom of OClO and the oxygen atom of water (top panel), the central carbon atom of acetonitrile (middle panel) and the central carbon atom of ethanol (bottom panel).

As is clear from Figure 8 and Table 2, the vibrational relaxation at the interface is significantly slower than in the bulk in all three solvents. The bulk rates are strongly energy dependent[28] and the same trend is observed at the surface. In bulk water, the relaxation time (inverse the rate constant) varies from around 4 ps at the highest energy excitation to near 13 ps at the lowest. At the interface, the rate is slower by a factor of 4 to a factor of 2 as we move to higher excitation energies. Similar behavior is observed in the other two liquids.

As discussed elsewhere,[28] the faster relaxation in water compared with the other two liquids is the result of a much higher density of liquid modes in the frequency range of the symmetric and antisymmetric modes of OClO (near 1000 cm^{-1}). These liquid modes are the consequence of the hydrogen bonding network in water. At the liquid surface, the decrease in solvent density reduces the friction on the solute vibrational modes and slows down the rate. In a recent paper,[26] we examined this question in detail for the relaxation of a diatomic solute at water surfaces. We found that in the case of a polar and nonpolar solute, the 50% liquid density at the surface results in a 3-fold slowing down effect on the rate of vibrational relaxation, while this slowing down is less pronounced if the solute is ionic. In all cases, the effect of the surface on the vibrational relaxation can be directly correlated with the change in the peak height of the radial distribution function. We see that the same applies to OClO at the surface of the three liquids considered in the present paper. Figure 9 shows the pair correlation function of the Cl atom (OClO) with the central solvent atom in each bulk liquid compared with that at the interface (calculated from separate equilibrium calculations). For each of the three liquids we find that $g_{bulk}(r_m)/g_{surface}(r_m) \approx 3$ where r_m is the peak position of the radial distribution function.

We conclude with a brief discussion of the intramolecular energy flow in OClO during the vibrational relaxation. Figures 10−12 give the average nonequilibrium kinetic energy of the three vibrational modes of OClO in the bulk and the surface of water (Figure 10), acetonitrile (Figure 11), and ethanol (Figure 12). We show the results following the highest excitation energy (37 kcal/mol), since the lower excitation cases show only

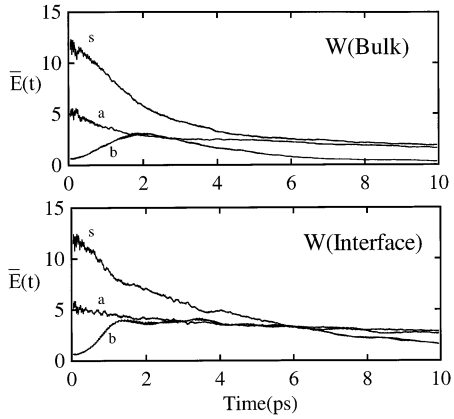

Figure 10. Average nonequilibrium vibrational kinetic energy (kcal/mol) partitioning into the different vibrational modes following the high (37 kcal/mol) vibrational excitation of OClO in bulk water (top panel) and at the water liquid/vapor interface (bottom panel) at 298 K. In each panel, the lines labeled "s", "a" and "b" correspond to the kinetic energy of the symmetric, anti-symmetric, and bending modes, respectively.

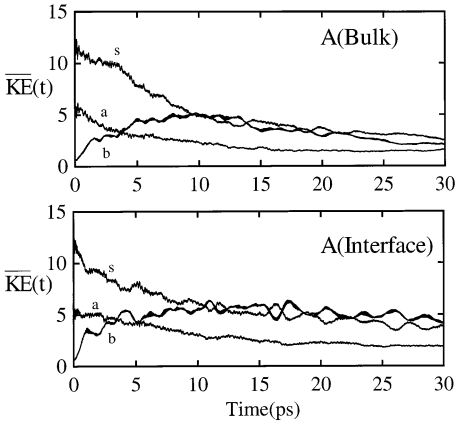

Figure 11. Same as Figure 10 (note the different time scale) for OClO in acetonitrile.

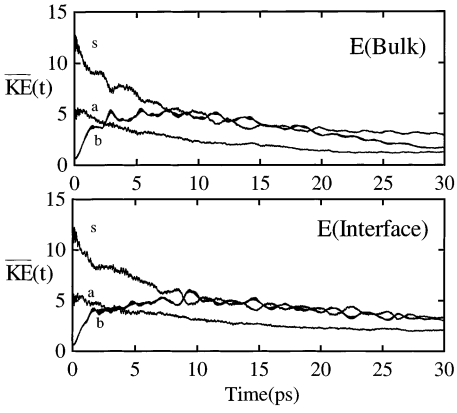

Figure 12. Same as Figure 11 for vibrational relaxation of OClO in ethanol.

minimal energy flow between the modes. In all cases, the relaxation of the symmetric (lines labeled "s") and anti-symmetric (lines labeled "a") modes results in significant energy flow into the bending mode (lines labeled "b"), which then relaxes on a time scale which is similar to that of the symmetric and anti-symmetric modes. Again, the relaxation is faster in the bulk than at the interface and in water than in the other two liquids (note the different time scales). We also observe, in ethanol and in acetonitrile, very pronounced periodic energy

flow between the bending and the symmetric mode, especially at the interface. This suggests that that these two modes are perturbed by the water to a greater degree than in the other two liquids and thus energy exchange back and forth between these two modes is less affected by the solvent in the case of acetonitrile and ethanol. The liquid perturbation is weaker at the interface and the oscillations are thus more pronounced in this case.

IV. Conclusions

The study of photodissociation and vibrational relaxation at the liquid surface region highlights two important characteristics of this medium: its narrow size and the reduced solvent density which gives rise to reduced solute solvation structure. The reduced solute solvation and the narrow region gives rise to nearly 100% cage escape following photodissociation and in most of the trajectories at least one of the dissociation fragments desorbs. The combination of both the reduced solvation and the smaller solvent density explain the fact that the vibrational relaxation of ground-state OClO is slower at the interface than in the bulk by a factor of 3 on average. These results are essentially independent of the nature of the liquid for the liquids considered in this work.

Acknowledgment. This work has been supported by a grant from the National Science Foundation (CHE-9981847). We are grateful for helpful discussions with Prof. Philip J. Reid.

References and Notes

(1) Ruhl, E.; Jefferson, A.; Vaida, V. *J. Phys. Chem.* **1990**, *94*, 2990.
(2) Baumert, T.; Herek, J. L.; Zewail, A. H. *J. Chem. Phys.* **1993**, *99*, 4430.
(3) Furlan, A.; Scheld, H. A.; Huber, J. R. *J. Chem. Phys.* **1997**, *106*, 6538.
(4) Lin, J. J.; Hwang, D. W.; Lee, Y. T.; Yang, X. M. *J. Chem. Phys.* **1998**, *108*, 10061.
(5) Esposito, A. P.; Stedl, T.; Jonsson, H.; Reid, P. J.; Peterson, K. A. *J. Phys. Chem. A* **1999**, *103*, 1748−1757.
(6) Dunn, R. C.; Simon, J. D. *J. Am. Chem. Soc.* **1992**, *114*, 4856.
(7) Dunn, R. C.; Flanders, B. N.; Simon, J. D. *J. Phys. Chem.* **1995**, *99*, 7360.
(8) Chang, Y. J. *J. Phys. Chem.* **1996**, *100*, 6406.
(9) Vaida, V.; Goudjil, K.; Simon, J. D.; Flanders, B. N. *J. Mol. Liq.* **1994**, *61*, 133.
(10) Graham, J. D.; Roberts, J. T.; Brown, L. A.; Vaida, V. *J. Phys. Chem.* **1996**, *100*, 3115.
(11) Thogersen, J.; Jepsen, P. U.; Thomsen, C. L.; Poulsen, J. A.; Byberg, J. R.; Keiding, S. R. *J. Phys. Chem. A* **1997**, *101*, 3317.
(12) Thogersen, J.; Thomsen, C. L.; Poulsen, J. A.; Keiding, S. R. *J. Phys. Chem. A* **1998**, *102*, 4186.
(13) Poulsen, J. A.; Thomsen, C. L.; Keiding, S. R.; Thogersen, J. *J. Chem. Phys.* **1998**, *108*, 8461.
(14) Philpott, M. J.; Charalambous, S.; Reid, P. J. *Chem. Phys. Lett.* **1997**, *281*, 1.
(15) Reid, P. J.; Esposito, A. P.; Foster, C. E.; Beckman, R. A. *J. Chem. Phys.* **1997**, *107*, 8262−8274.
(16) Hayes, S. C.; Philpott, M. J.; Reid, P. J. *J. Chem. Phys.* **1998**, *109*, 2596.
(17) Philpott, M. J.; Hayes, S. C.; Reid, P. J. *Chem. Phys. (Netherlands)* **1998**, *236*, 207−224.
(18) Thomsen, C. L.; Philpott, M. P.; Hayes, S. C.; Reid, P. J. *J. Chem. Phys.* **2000**, *112*, 505.
(19) Foster, C. E.; Barham, B. P.; Reid, P. J. *J. Chem. Phys.* **2001**, *114*, 8492−8504.
(20) Philpott, M. P.; Hayes, S. C.; Thomsen, C. L.; Reid, P. J. *Chem. Phys.* **2001**, *263*, 389−400.
(21) Fidder, H.; Tschirschwitz, F.; Duhr, O.; Nibbering, E. T. J. *J. Chem. Phys.* **2001**, *114*, 6781−6794.
(22) Vaida, V.; Simon, J. D. *Science* **1995**, *269*, 1443.
(23) Lanzendorf, E. J.; Kummel, A. C. *Geophys. Res. Lett.* **1996**, *23*, 1521−1524.
(24) Graham, J. D.; Roberts, J. T.; Anderson, L. D.; Grassian, V. H. *J. Phys. Chem.* **1996**, *100*, 19551.
(25) Vieceli, J.; Chorny, I.; Benjamin, I. *J. Chem. Phys.* **2001**, *115*, 4819.
(26) Vieceli, J.; Chorny, I.; Benjamin, I. *J. Chem. Phys.* **2002**, *117*, 4532.
(27) Vieceli, J.; Chorny, I.; Benjamin, I. *Chem. Phys. Lett.* **2002**, *364*, 446.
(28) Chorny, I.; Vieceli, J.; Benjamin, I. *J. Chem. Phys.* **2002**, *116*, 8904.
(29) Chorny, I.; Vieceli, J.; Benjamin, I. *J. Chem. Phys.* **2002**, *116*, 8930.
(30) Peterson, K. A. *J. Chem. Phys.* **1998**, *109*, 8864.
(31) Huber, K. P.; Herzberg, G. *Constants of Diatomic Molecules*; Van Nostrand Reinhold: New York, 1979.
(32) Nicholis, R. W. *J. Atmos. Sci.* **1975**, *32*, 856.
(33) Pettersson, L. G. M.; Langhoff, S. R.; Chong, D. P. *J. Chem. Phys.* **1986**, *85*, 2836.
(34) Benjamin, I. Molecular dynamics methods for studying liquid interfacial phenomena. In *Modern Methods for Multidimensional Dynamics Computations in Chemistry*; Thompson, D. L., Ed.; World Scientific: Singapore, 1998; p 101.
(35) Edwards, D. M. F.; Madden, P. A.; McDonald, I. R. *Mol. Phys.* **1984**, *51*, 1141.
(36) Jorgensen, W. L. *J. Phys. Chem.* **1986**, *90*, 1276.
(37) Kuchitsu, K.; Morino, Y. *Bull. Chem. Soc. Jpn.* **1965**, *38*, 814.
(38) Herzberg, G. *Molecular Spectra and Molecular Structure*, Vol. II; Van Nostrand: New York, 1945.
(39) Hansen, J.-P.; McDonald, I. R. *Theory of Simple Liquids*, 2nd ed; Academic: London, 1986.
(40) Berendsen, H. J. C.; Postma, J. P. M.; Gunsteren, W. F. V.; Hermans, J. In *Intermolecular Forces*; Pullman, B., Ed.; D. Reidel: Dordrecht, 1981; p 331.
(41) Benjamin, I.; Whitnell, R. M. *Chem. Phys. Lett.* **1993**, *204*, 45.
(42) Benjamin, I.; Barbara, P. F.; Gertner, B. J.; Hynes, J. T. *J. Phys. Chem.* **1995**, *99*, 7557.
(43) Li, Z. M.; Fang, J. Y.; Martens, C. C. *J. Chem. Phys.* **1996**, *104*, 6919.
(44) Wang, H.; Borguet, E.; Eisenthal, K. B. *J. Phys. Chem.* **1997**, *101*, 713.
(45) Benjamin, I. *Chem. Phys. Lett.* **1998**, *287*, 480.